Effect of spatial variability on the slope stability using random field numerical limit analyses

Kiyonobu Kasama

Division of Civil and Structural Engineering, Faculty of Engineering, Kyushu University, Fukuoka, Japan

774 Motooka, Nishi-ku, Fukuoka 819-0395 JAPAN

Tel:+81-92-802-3385 Fax:+81-92-802-3383

kasama@civil.kyushu-u.ac.jp

Andrew J. Whittle

Department of Civil and Environmental Engineering, Massachusetts Institute of Technology, MA, USA

Effect of spatial variability on the slope stability using random field numerical limit analyses

This paper presents a probabilistic approach to evaluating the geotechnical stability problem by incorporating the stochastic spatial variability of soil property within the numerical limit analyses. The undrained shear strength and unit weight of soil are treated as a random field which is characterized by a log-normal distribution and a spatial correlation length. The current calculations use a Cholesky Decomposition technique to incorporate these random properties in numerical limit analyses. The Random Field Numerical Limit Analyses are applied to evaluate effects of spatial variability of soil property on the slope stability and failure mechanism of slope. Monte Carlo iterations are then used to interpret the slope reliability and the dimension for collapsed slope for selected ranges of the coefficient of variation in soil property and the ratio of correlation length to slope height. Finally, the variation in the dimension of collapsed slope is examined in terms of the variability of slope reliability.

Keywords: slope stability; limit analysis; Monte Carlo method; failure mode

Introduction

The spatial variability and uncertainty of soil parameters such as unit weight and shear strength should be treated rationally and quantitatively to evaluate the safety of slope failure. The reliability design based on the probabilistic and statistic theory can evaluate the safety of slope as a liability index and failure probability. Sakurai & Doi (1983) and Mellah et al. (2000) proposed the stochastic finite element method for the stability problem of slope and embankment. Husein Malkawi et al. (2000) performed the reliability design for slope stability based on the First Order Second Moment method (FOSM) and Monte Carlo iteration. For the practical application of reliability design, Christian et al. (1994) and El-Ramly et al. (2002) reported appropriate safety factor for a large scale embankment on saturated clayey ground considering the testing error, statistical estimation error and spatial variability of soil parameters. Moreover, Griffiths & Fonton (2004) clarified the reliability of slope using the random field finite element method and Monte Carlo iteration.

This paper presents a Random Field Numerical Limit Analyses to evaluating the geotechnical stability problem by incorporating the stochastic spatial variability of soil property within the numerical limit analyses. The Random Field Numerical Limit Analyses are applied to evaluate effects of spatial variability of soil property on the slope stability and failure mechanism of slope. Monte Carlo iterations are then used to interpret the slope reliability and the dimension for collapsed slope for selected ranges of the coefficient of variation in soil property and the ratio of correlation length to slope height. Finally, the variation in the dimension of collapsed slope is examined in terms of the variability of slope reliability

Random Field Numerical Limit Analyses

Numerical limit analyses

The Numerical Limit Analyses (NLA) used in this study were based on 2-D, plane strain linear programming formulations of the Upper Bound (UB) and Lower Bound (LB) theorems for rigid, perfectly plastic materials presented by Sloan & Kleeman (1995) and Lyamin & Sloan (2002). The upper-bound formulation assumes linear variations in the unknown velocities (u_x, u_y) within each triangular finite element. Nodes are unique to each element and hence, the edges between elements represent planes of velocity discontinuities. Plastic volume change and shear distortion can occur within each element as well as along velocity discontinuities. The kinematic constraints are defined by the compatibility equations and the condition of associated flow (based on an appropriate linearization of the Tresca criterion) within each element and along the velocity discontinuities between elements. The external applied load can be expressed as a function of unknown nodal velocities and plastic multiplier rates. The upper bound on the collapse load can then be formulated as a linear programming problem, which seeks to minimize the external applied load using an active set algorithm (after Sloan and Kleeman, 1995).

Recent numerical formulations of upper and lower bound limit analyses for rigid perfectly plastic materials, using finite element discretization and linear or non-linear programming methods, provide a practical, efficient and accurate method for performing geotechnical stability calculations. For example, Ukritchon et al. (1998) proposed a solution to the undrained stability of surface footings on non-homogeneous and layered clay deposits under the combined effects of vertical, horizontal and moment loading to a numerical accuracy of +/- 5%. One of the principal advantages of NLA is that cohesion and friction angle were only input parameters. Hence, NLA provides a more convenient method of analyzing stability problems than conventional displacement-based finite element methods which also require the specification of stiffness parameters and simulation of the complete non-linear load-deformation response up to collapse (e.g., Ukritchon et al., 1998; Kasama & Whittle, 2012; Huang et al., 2013).

Figure 1 illustrates a typical finite element mesh used for two dimensional slope stability program with the slope angle of 45^{o}. The model considers a soil layer with depth z/H = 1.0 and the width x/H =5.0, where H is the height of the slope. The dimension of square mesh divided into four quarter elements is 0.1 H. The mean undrained shear strength μ_c is 100 kPa and mean unit soil weight μ_γ is 18 kN/m^3. The boundary conditions are rollers on the left and right vertical boundaries, and full fixity at the base. The number of elements is 1800 and the number of node is 5400. It took six minutes to complete one irritation of Monte Carlo simulation including generate the random field.

Random field iterations

The effects of inherent spatial variability are represented in the analyses by modeling the undrained shear strength, c_u, and unit weight, γ, as a homogeneous random field (Vanmarcke, 1984). The undrained shear strength and unit weight are assumed to have an underlying log-normal distribution with mean, μ_c and μ_γ, and standard deviation, σ_c and σ_γ, and an isotropic scale of fluctuation (also referred to as the correlation length), θ_c and θ_γ. Current iteration assumes that correlation length of unit weight θ_γ is similar to that of undrained shear strength θ_c. Following Griffiths & Fenton (2004) the current analyses present results based on assumed values of the ratio of the correlation length to slope height, $\Theta = \theta_c / H = \theta_\gamma / H$ as an input parameter. The similar correlation length lies with the range of the undrained shear strength and unit weight.

The mean and standard deviation of log c_u and log γ are readily derived from μ_c and σ_c and μ_γ and σ_γ as follows (e.g., Baecher & Christian, 2003):

$$\sigma_{\ln c} = \sqrt{\ln(1+\sigma_c^2)}\,;\ \sigma_{\ln\gamma} = \sqrt{\ln(1+\sigma_\gamma^2)} \qquad (1)$$

$$\mu_{\ln c} = \ln\mu_c - \frac{1}{2}\sigma_{\ln c}^2\,;\ \mu_{\ln\gamma} = \ln\mu_\gamma - \frac{1}{2}\sigma_{\ln\gamma}^2 \qquad (2)$$

The spatial variability is incorporated within the NLA meshes by assigning the undrained shear strength, c_i, and unit weight, γ_i, corresponding to the ith element:

$$c_i = \exp(\mu_{\ln c} + \sigma_{\ln c} \cdot G_i) \qquad (3.1)$$

$$\gamma_i = \exp(\mu_{\ln\gamma} + \sigma_{\ln\gamma} \cdot G_i) \qquad (3.2)$$

where G_i is a random variable that is linked to the spatial correlation length, θ_c and similar G_i is used to calculate c_i and γ_i in this study. Namely, it is assumed that unit weight of ith element, γ_i was assumed to be perfectly correlated with the undrained shear strength of ith element, c_i, which agrees with experimental findings that there is strong correlation between undrained shear strength and unit weight of soil. Values of G_i are obtained using a Cholesky Decomposition technique (Matthies et al., 1997; Baecher and Christian, 2003; Kasama et al., 2006; Kasama and Whittle, 2011) using an isotropic Markov function which assumes that the correlation decreases exponentially with distance between two points i, j:

$$\rho(x_{ij}) = \exp(-2x_{ij}/\theta) \qquad (4)$$

where ρ is the correlation coefficient between two random values of c_u and γ at any points separated by a distance $x_{ij} = |x_i - x_j|$ where xi is the position vector of i (located at the center of element i in the finite element mesh).

This coefficient can be used to generate a correlation matrix, $\boldsymbol{K}$, which presents the correlation coefficient between each of the elements used in the NLA finite element meshes:

$$\boldsymbol{K} = \begin{bmatrix} 1 & \rho_{12} & \cdots & \rho_{1n_e} \\ \rho_{12} & 1 & \cdots & \rho_{2n_e} \\ \vdots & \vdots & \ddots & \\ \rho_{1n_e} & \rho_{2n_e} & \cdots & 1 \end{bmatrix} \quad (5)$$

where ρ_{ij} is the correlation coefficient between element i and j, and n_e is the total number of elements in the mesh.

The matrix $\boldsymbol{K}$ is positive definite and hence, the standard Cholesky Decomposition algorithm can be used to factor the matrix into upper and lower triangular forms, $\boldsymbol{S}$ and $\boldsymbol{S}^{\mathrm{T}}$, respectively:

$$\boldsymbol{S}^{\boldsymbol{T}}\boldsymbol{S} = \boldsymbol{K} \quad (6)$$

The components of $\boldsymbol{S}^{\mathrm{T}}$ are specific to a given finite element mesh (for either UB or LB) and selected value of the correlation length, $\theta_{\ln c}$.

The vector of correlated random variables, $\boldsymbol{G}$ (i.e., $\{G_1, G_2,\ldots, G_{ne}\}$, where G_i specifies the random component of the undrained shear strength and unit weight in element i, eqn. 3) can then be obtained from the product:

$$\boldsymbol{G} = \boldsymbol{S}^{\boldsymbol{T}}\boldsymbol{R} \quad (7)$$

where $\boldsymbol{R}$ is a vector of statistically independent, random numbers $\{r_1, r_2,\ldots, r_{ne}\}$ with a standard normal distribution (i.e., with zero mean and unit standard deviation).

The current implementation implicitly uses the distance between the centroids to define the correlations between undrained shear strengths and unit weights in adjacent elements. This is an approximation of the random field, which involves the integral of the correlation function over the areas of the two elements. Noted that the effects of the mesh refinement an element size on random field were presented by Kasama et al. (2012).

Values of the random variable vector ***R*** are re-generated for each realization in a set of Monte Carlo iterations. Figure 1 illustrates the spatial distribution of undrained shear strength obtained for a typical mesh for one example iteration with input parameters μ_c =100kPa, COV_c = (σ_c/μ_c) = 0.4 and Θ = 1.0. The lighter shaded regions indicate areas of higher shear strength. A parametric study has been performed using the ranges listed in Table 1. The angle of slope is 30^{o}, 45^{o} and 60^{o}. It is noted that input coefficient of variability of undrained shear strength, COV_c, ranges from 0.2 to 1.0 while input coefficient of variability of unit weight, COV_γ, is fixed at 0.1 because the spatial variability of unit weight is generally less than that of shear strength (e.g. Phoon & Kulhawy, 1999). Normalized correlation length Θ ranges from 0.25 to 4.0 in addition to very small correlation length which is corresponding that the strength of elements was randomly determined (called "Random" for input parameter in this paper). Although horizontal correlation length is generally larger than vertical one for naturally deposited soils, horizontal correlation length assumed to be identical to vertical correlation length in this study. This assumption expected to induce the instability of slope. For example, Al-Bittar & Soubra investigated the effect of anisotropic correlation structure of shear strength on the bearing capacity problems suggesting that the variability of the ultimate bearing capacity for a given vertical correlation length decreases when the horizontal correlation length increases. For each set of parameters, a series of 1000 Monte Carlo iterations have been performed. In this paper, the result of UB calculations is mainly used to examine the failure dimension of collapsed slope in addition to evaluate the slope stability.

Numerical Result

Stochastic stability number

In order to evaluate the stochastic property of slope stability with the spatial variability of soil property, the computed Cousins' stability number for slope can then be reported for each iteration, i, of the random field, N_{si}, as follows (Cousins 1978):

$$N_{si} = \frac{F_{si} \cdot \mu_\gamma \cdot H}{\mu_c} \tag{8}$$

where F_{si} is a conventional safety factor of slope for ith iteration. It is noted that the Cousins' stability number is the reciprocal of Taylar's stability, which indicates that a safety factor for slope is a linear function of Cousins' stability number, namely, large Cousins' stability number means large safety factor of slope. That is the reason why Cousins' stability number for slope was used in this study. In addition, the Cousins' stability number for a given inclined angle β of slope shows constant value meaning that safety factor of slope F_s, soil unit weight γ, slope height H and undrained shear strength c are balanced. For example, increase in slope height H for a slope with similar strength c, unit weight γ and the inclined angle β cause reduction of safety factor of slope F_s to maintain the constant value of Cousins' stability number. The Cousins' stability number N_{sDet} for homogeneous slope of 45^o with μ_c and μ_γ is 5.57, which is equivalent to 5.52 and 5.59 reported by Taylor (1948) and Terzaghi & Peck (1967) respectively. Hence, the mean, μ_{Ns}, and standard deviation, σ_{Ns}, of the stability number are recorded through each set of Monte Carlo iterations, as follows:

$$\mu_{N_s} = \frac{1}{n}\sum_{i=1}^{n} N_{s_i} \; ; \; \sigma_{N_s} = \sqrt{\frac{1}{n-1}\sum_{i=1}^{n}(N_{s_i} - \mu_{N_s})^2} \tag{9}$$

Figure 2 illustrates one set of results for the case with n = 1000, Θ = 1.0, COV_γ = 0.1 and COV_c = 0.2, 0.6 and 1.0. The results confirm that the accumulative mean and standard deviation of N_s both become stable within 1000 iterations and hence, reliable statistical interpretation of the data can be obtained from this set of iterations. Several studies (e.g., Phoon et al., 2008) have performed to determine an appropriate number of Monte Carlo iteration combining reasonable accuracy of the results in terms manageable computational efforts for a large parametric study.

Figure 3 shows a 20-bin histogram of the stability number from one complete series of Monte Carlo iterations with COV_c = 1.0 and Θ= 0.25 and 1.0. Based on χ^2 goodness-of-fit tests, it is concluded that normal or log-normal distribution functions can be used to characterize the stability number at a 5% significance level.

Mean and standard deviation of stability number

In order to evaluate the effect of the slope dimension on the stability for slope with the spatial variability of soil property, Figure 4 shows the relationships between mean stability number μ_{Ns} for $\Theta = 1.0$ and slope angle. Noted that the result of mean stability number for the slope with uniform strength ($COV_c = 0$ and $COV_\gamma = 0.1$) is also shown in Figure 4. The stability number for a given COV_c decreases linearly with increasing slope angle while the decrease rate of stability number against slope angle is similar irrespective of COV_c.

In order to examine the variability of stability number, Figure 5 shows the relationships between $COV_{Ns} = (\sigma_{Ns}/\mu_{Ns})$ and COV_c for a given Θ. For the slope with elements having randomly determined strength (Θ = Random), COV_{Ns} indicates constant value of 0.1 irrespective of COV_c, which is considered to be attributed from the variability of unit weight ($COV_c = 0.1$). Except for Θ = Random, COV_{Ns} for a given Θ increases linearly with increasing COV_c while the increase rate of COV_{Ns} increases from $\Theta = 0.25$ to $\Theta = 2.0$. It can be emphasized that the magnitude of COV_{Ns} is relatively small at most 0.25 even if the magnitude of COV_c is large ($COV_c = 1.0$) suggesting that the variability of strength averages locally along a slip surface of slope.

Figure 6 shows the mean stability number μ_{Ns} against normalized correlation length Θ for a given slope angle and $COV_c = 0.4$ and 0.8. The mean stability number μ_{Ns} increases with increasing Θ irrespective of slope angle and COV_c while the increase rate increases as COV_c increases. For example, the mean stability number μ_{Ns} for $COV_c = 0.8$ increases 40% when Θ change from 0 to 4.0. It can be seen that the magnitude of Θ affect greatly the mean stability number particular for the slope with large spatial variability.

Figure 7 shows the relationships between COV_{Ns} = (σ_{Ns}/μ_{Ns}) and Θ for COV_c = 0.4 and 0.8. COV_{Ns} indicates the maximum value at Θ = 2.0. COV_{Ns} for slope angle = 60^o indicates larger value compared with those for slope angle = 30^o and 45^o. It can be suggested that the variability of stability number becomes large when the slope angle is large. This is because the variability of undrained shear strength along the slip surface become small when the length of slip surface becomes short with decreasing slope angle, namely the local averaging of undrained shear strength occurs along the slip surface.

Reduction of stability number due to spatial variability

Figures 8 summarize the reduction ratio of mean stability number obtained by equation (9) to deterministic solution for homogeneous slope with μ_c and μ_γ, $R_{Ns} = \mu_{Ns}/N_{sDet}$ (where N_{sDet} = 5.57) for combinations of the input parameters (COV_c, Θ). In general, $R_{Ns} < 1$ and hence spatial variability causes a reduction in the expected slope stability. The trends show that the largest reductions in μ_{Ns} occur when the coefficient of variation is high and/or the correlation length is small.

Figure 9 shows the reduction ratio of accumulative mean stability number and 99% lower confidence bound of stability number against normalized correlation length Θ. It is noted that the 99% lower confidence bound of stability number, $R_{Ns99\%} = N_{sl99\%}/N_{sDet}$, was calculated where $N_{sl99\%}$ is estimated by assuming a log-normal distribution with μ_{Ns} and σ_{Ns}. Accumulated mean stability number gradually increases with increasing Θ while the increase rate slightly increase as COV_c increases. The 99% lower confidence bound of stability number shows a minimum value at Θ = 1.0. Moreover, the difference of the 99% lower confidence bound of stability number for a given COV_c is less than 10 % for $0 < \Theta < 4.0$ suggesting that correlation length is less important among input parameters representing the spatial variability of slope.

Failure Mechanism

Figures 10 illustrate typical failure mechanisms from a series of UB calculations for slope with the inclined angle of 45°, COV_c = 0.4 and Θ = 1.0. Figure 10a) shows deformed FE mesh and the distribution of input shear strength. Figure 10b) shows dissipated energy together with the vectors of the computed velocity field. Figures 11 illustrate failure mechanisms for similar slope with uniform strength and unit weight. Taylor proposed that a conventional failure mechanism for the slope the inclined angle of 45° is a deep failure mechanism tangent to the base as shown in Figures 11. On the other hand, due to the random field, close inspection shows that the computed failure mechanisms find paths of least resistance, passing through weaker soil elements in the slope. It can be seen that there is a well defined toe failure passing through the weak soil zone near the slope toe and there is a concentration of dissipated energy at the toe of slope. It is suggested that the location of weak soil elements in the slope affects failure mechanism of slope.

In order to evaluate a dimension of slope failure statistically, Figures 12 shows a histogram of the depth and width of collapsed slope for a given COV_c and the inclined angle of slope β. It is noted that the width of slope failure W_{Det} for uniform strength, unit weight and the inclined angle β of 30°, 45°, and 60° are 6.0 H, 5.0 H and 3.6 H respectively while the depth of slope failure D_{Det} for uniform strength and unit weight is 2.0 H irrespective of the inclined angle of 30°, 45°, and 60°. The depth and width of slope failure for β = 30° and the COV_c = 0.2, which is small spatial variability, indicates the maximum frequency at 2.0 H and 5.0 H respectively and the frequency decreases as the width decreases. However, the frequency of the depth less than 2.0 H and width less than 5.0 H increases when COV_c increases. Therefore, the dimension of collapsed slope for COV_c = 0.6 and 1.0 indicates more complex distribution, particularly the frequency of the width and depth becomes uniform distribution as the inclined angle of slope becomes large. In addition, it is interesting point that the width of slope failure for β = 30° includes larger width then 3.6 H, which is the width of slope failure for uniform strength, unit weight and the inclined angle of 60°. For the depth of slope failure, the frequency of 2.0 H is large irrespective of COV_c and β, meaning that the slope failure shows a deep failure mechanism tangent to the base (base failure). In addition, the frequency of 1.0 H increases with increasing β and COV_c especially for $\beta = 60°$. The depth of 1.0 H for slope failure means that slope failure shows a toe failure mechanism passing the toe of slope. It can be expected that failure mechanism for steep slope shifts from a base failure to toe failure with the increasing spatial variability. Finally, it is suggested that the depth and width of slope failure decrease with increasing spatial variability of soil unit weight and shear strength, namely a slope with a large spatial variability causes a local failure resulting from the pre-failure of weak soil elements.

Figure 13 shows the relationships between the depth and width for collapsed slope with β = 30 °, 45° and 60 °, Θ = 1.0 and COV_γ=0.1. The square range indicates the coordinates of mean width μ_W +/- standard deviation σ_W and the mean depth μ_D +/- standard deviation σ_D for a given COV_c because an original relationships between the depth and the width of slope failure scatter remarkably. The center of square decreases with increasing COV_c and the area of square range extends with increasing COV_c, which is suggesting that the dimension of collapsed slope becomes small and local as the spatial variability of soil property increases while the variability of the dimension increases as the spatial variability of soil property increases. In addition, the area of square range extends with increasing β, which is suggesting that there is a wide variation in the dimension of collapsed slope as the angle of slope increases.

In order to examine effects of spatial variability on the failure mechanism for slope, Figure 14 shows the relationships between mean width of failure zone and mean depth of failure surface for a given β obtained from a series of Monte Carlo iteration. It is noted that the width and depth of failure zone in horizontal and vertical axis respectively are normalized by those for homogeneous slope. For the inclined angle of slope of 30°, there is a linear relationships between depth and width irrespective of values of Θ and the dimension of slope failure decreases with increasing COV_c

suggesting that small slope failure is generated due to the spatial variability of mechanical property. For the inclined angle of slope of 45^{o}, it can be seen that the mean width and depth of failure zone for slope with spatial variability decreases with increasing COV_c and Θ. It can be suggested that the spatial variability of soil property greatly affects to failure mechanism of slope. Moreover, the location of weak soil elements in slope is important to local failure of slope and the scale of slope failure decreases with increasing the magnitude of spatial variability of soil property. For the inclined angle of slope of 60^{o}, the depth for spatially variable slope decreases sharply up to less than 80% of that for uniform slope. It can be emphasized that small and local failure mechanism induces for spatially variable slope as the inclined angle of slope increases.

In order to evaluate stability number for spatially variable slope in terms of the failure mechanism, the relationships between stability number and the width of slope failure is shown in Figure 15 for β = 30^{o}, 45^{o} and 60^{o}, Θ = 1.0 and COV_{γ}=0.1. The square range of mean stability number μ_{Ns} +/- standard deviation σ_{Ns} and the mean width μ_W +/- standard deviation σ_W for a given COV_c is shown in this Figure because an original relationships between stability number and the width of slope failure scatter remarkably. The area of square range extends with increasing COV_c, which is suggesting that the stability for spatially variable slope is closely related to the failure mechanism and slope with a large spatial variability tends to induce a local and diverse failure.

Failure Probability and Safety Factor

In order to link obtained probabilistic results to conventional evaluation for slope stability using safety factor, the relationship between the probability of slope failure and mean safety factor of slope for a given COV_c and the inclined angle of slope β are shown in Figure 16 together with results of conventional FOSM by Matsuo (1984). The probability of slope failure became over 0.5 even for the mean safety factor of 1.0 because the mean stability number for slope with spatial variability is less than that for homogeneous slope as shown in figure 4. The probability of slope failure for given COV_c and Θ decreases drastically as F_s increases compared to results of conventional FOSM. Moreover, the probability of slope failure for a given F_s increases with decreasing Θ and increasing β, which is suggesting that the potential of local slope failure increases with decreasing Θ and increasing β. In addition, the probability difference among different becomes small as the inclined angle of slope increases. It can be characterized that the numerical limit analyses incorporated with the random field theory is useful for representing local slope failure induced by the spatial variability of soil property.

Conclusions

This paper has presented initial results from a probabilistic study on the slope stability problem using random field numerical limit analyses and Monte Carlo iteration. The main conclusions are as follows:

1) The stability number of slope considering the spatial variability of shear strength and unit soil weight can be characterized by both normal and log-normal distribution functions with 5% significance level.

2) The stability number decreases linearly with increasing the coefficient of variation in the shear strength while the 99% lower confidence bound of stability number shows a minimum value at Θ = 1.0.

3) The failure zone of slope can be localized by generating failure surface through weak soil elements. The stability for spatially variable slope is closely related to the failure mechanism and slope with a large spatial variability tends to induce a local and diverse failure. It can be emphasized that small and local failure mechanism induces for spatially variable slope as the inclined angle of slope increases because failure mechanism for steep slope shifts from a base failure to toe failure with the increasing spatial variability.

4) The probability of slope failure for given COV_c and Θ decreases drastically as F_s increases compared to results of conventional FOSM. The probability of slope failure for a given F_s increases with decreasing Θ, and increasing the inclined angle of slope β which is suggesting that the potential of local slope failure increases with decreasing Θ and increasing the inclined angle of slope β.

Acknowledgment

A grateful acknowledgment is made to Professors Hidetoshi Ochiai, Kouki Zen and Noriyuki Yasufuku of Kyushu University for their helpful advice and encouragement. This research was supported by the Grant-in-Aid for Scientific Research (B), JSPS KAKENHI Grant Number 25289149.

Reference

Al-Bittar, T. and Soubra, A.-H. 2013. Bearing capacity of strip footings on spatially random soils using sparse polynomial chaos expansion. Int. J. Numer. Anal. Meth. Geomech., 37: 2039–2060. doi: 10.1002/nag.2120

Baecher, G.B. & Christian, J.T. 2003. Reliability and statistics in geotechnical engineering, John Wiley & Sons, Ltd.

Christian, J.T., Ladd, C.C. & Baecher, G.B. 1994. Reliability Applied to Slope Stability Analysis, J. Geotech. ASCE, Vol. 120, No. 12, pp.2180-2207.

Cousins, B. F. 1978. Stability charts for simple earth slopes. J. Geotech. Engng, ASCE 104, No. 2, pp.267-279.

El-Ramly, H., Morgenstern, N.R. & Cruden, D.M. 2002. Probabilistic slope stability analysis for practice, Can. Geotech. J., Vol. 39, pp.665-683.

Griffiths, D.V. & Fenton, G.A. 2004. Probabilistic Slope Stability Analysis by Finite Elements, J.

Geotech and Geoenvi. Eng., ASCE, Vol.130, No.5, pp.507-518.

Huang, J., Lyamin, A.V., Griffiths, D.V., Krabbenhoft, K. & Sloan, S.W. 2013. Quantitative risk assessment of landslide by limit analysis and random fields, Computers and Geotechnics, Vol.53, pp.60-67.

Husein Malkawi, A.I., Hassan, W.F. & Abdulla, F.A. 2000. Uncertainty and reliability analysis applied to slope stability, Structural Safety, Vol.22, pp.161-187.

Kasama, K. & Whittle, A.J. 2011. Bearing Capacity of Spatially Random Cohesive Soil Using Numerical Limit Analyses, J. Geotech and Geoenvi. Eng., ASCE, Vol.137, No.11, pp. 989-996.

Kasama, K., Whittle, A.J. & Zen, K. 2012. Effect of Spatial Variability on Bearing Capacity on Cement-Treated Ground, Soils and Foundations, Vol.52, No.4, pp.600-619.

Lyamin, A.V. & Sloan, S.W. 2002. Lower bound limit analysis using non-linear programming, Intl. Journal for Numerical Methods in Engineering, Vol.55, No.5, pp.573-611.

Matthies, H. G., Brenner, C. E., Bucher, C. G. and Soares C. G. 1997. Uncertainties in probabilistic numerical analysis of structures and solids - stochastic finite elements, Structural Safety, 19(3), 283-336.

Matsuo, M. 1984. Geotechnical Engineering -Concept and Practice of Reliability-based Design-, Gihodo Shuppan, Ltd.

Mellah, R., Auvinet, G. & Masrouri, F. 2000. Stochastic finite element method applied to non-linear analysis of embankments, Probabilistic Engineering Mechanics, Vol.15, pp.251-259.

Phoon, K. K. 2008. Numerical recipes for reliability analysis – a primer, Chapter 1 of Reliability-Based Design in Geotechnical Engineering: Computations and Applications edited by Phoon, K.K., Taylor & Francis.

Phoon, K. K. & Fred H Kulhawy, F. H. 1999. Characterization of geotechnical variability, Canadian Geotechnical Journal, Vol.36, No.4, pp.612-624.

Sakurai, S. & Doi, Y. 1983. Reliability analysis of slope by finite element method, J. of Japan Society of Civil Engineers, JSCE, Vol.330, pp.87-97.

Sloan, S.W. & Kleeman, P.W. 1995. Upper bound limit analysis using discontinuous velocity fields, Comput. Methods Appl. Mech. Eng., Vol.127, pp.293-314.

Taylor, D.W. 1948. Fundamentals of soil mechanics, John Wiley and Sons, Ins., New York.

Terzaghi, K. & Peck, R.B. 1967. Soil mechanics in engineering practices, 2nd edition, John Wiley & Sons.

Ukritchon, B., Whittle, A.J. & Sloan, S.W. 1998. Undrained limit analyses for combined loading of strip footing on clay, J. Geotech. Eng., ASCE, Vol.124, No.3, pp.265-276.

Vanmarcke, E.H. 1984. Random fields: Analysis and synthesis, MIT press, Cambridge, Mass.

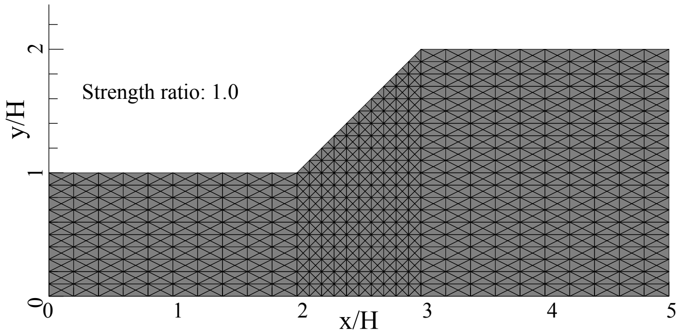

a) Mesh for slope stability with uniform strength

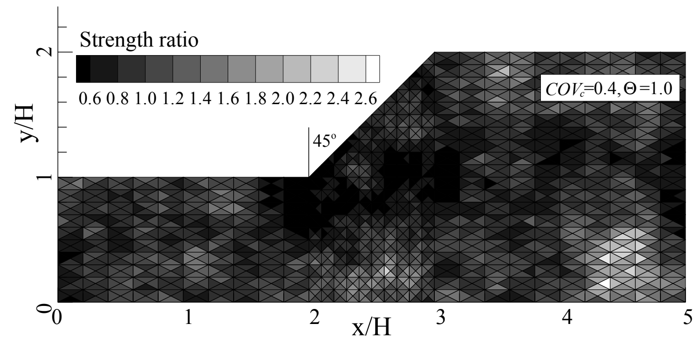

b) Mesh considering the spatial variability of shear strength

Figure 1. Typical mesh for slope stability.

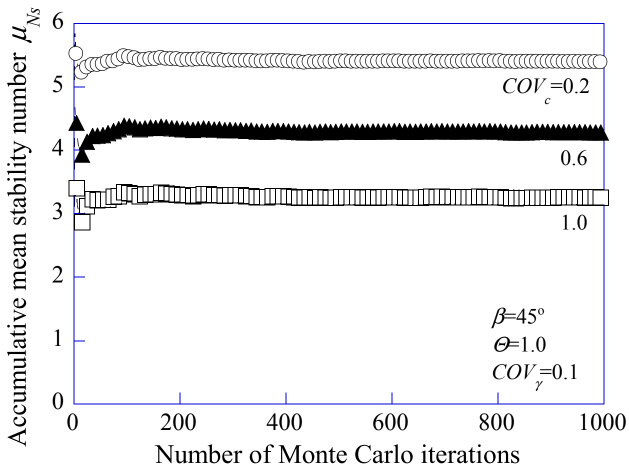

a) Accumulative mean stability number

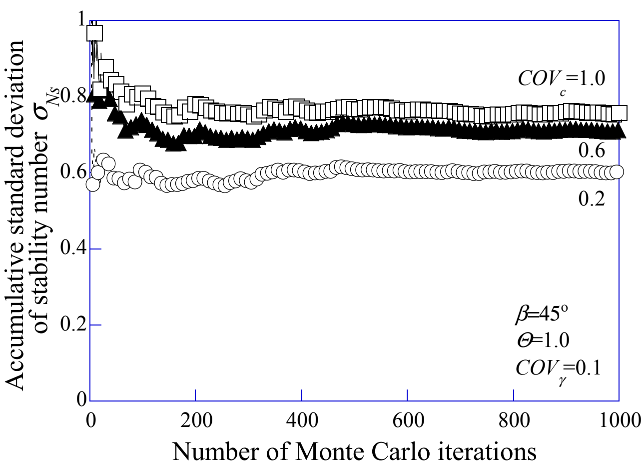

b) Accumulative standard deviation of stability number

Figure 2. Accumulative mean and standard deviation of stability number in Monte Carlo iterations.

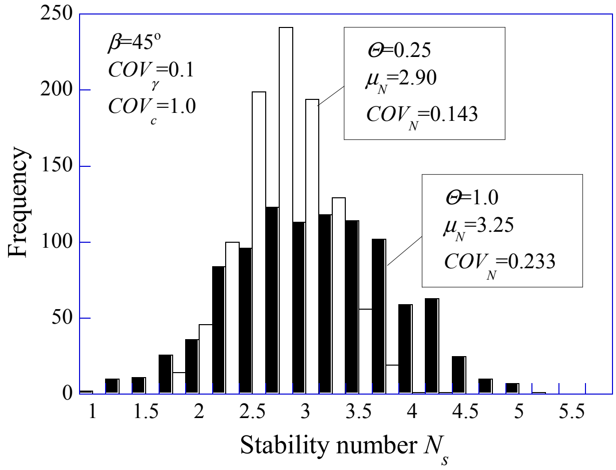

Figure 3. Histogram of stability number for slope.

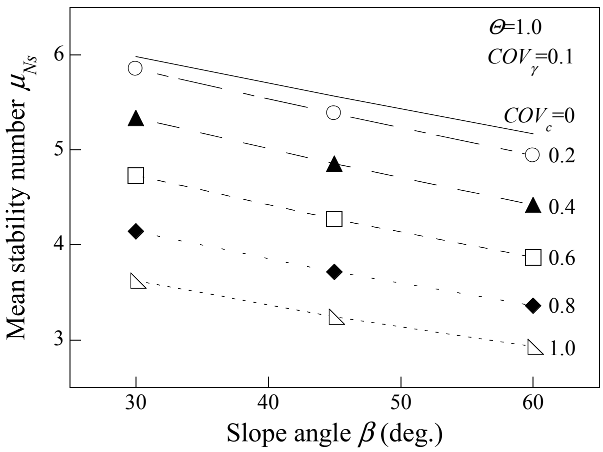

Figure 4 Mean stability factor and slope angle.

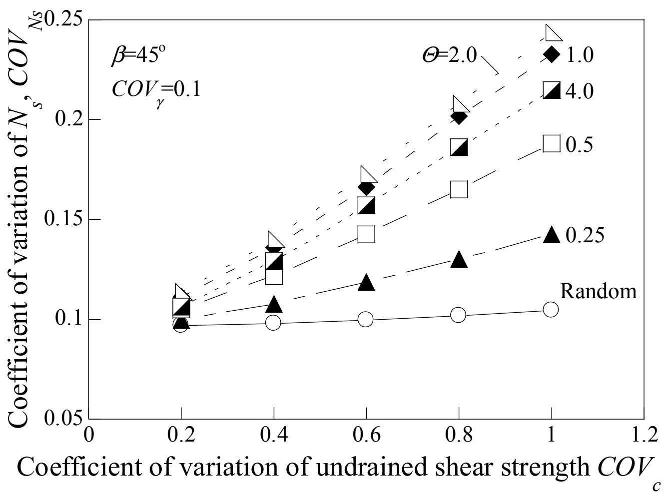

Figure 5 *COV* of slope stability number and COV_c.

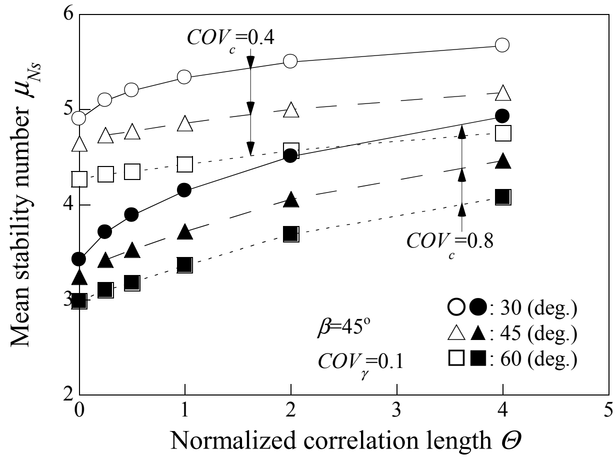

Figure 6 Mean stability number and normalized correlation length.

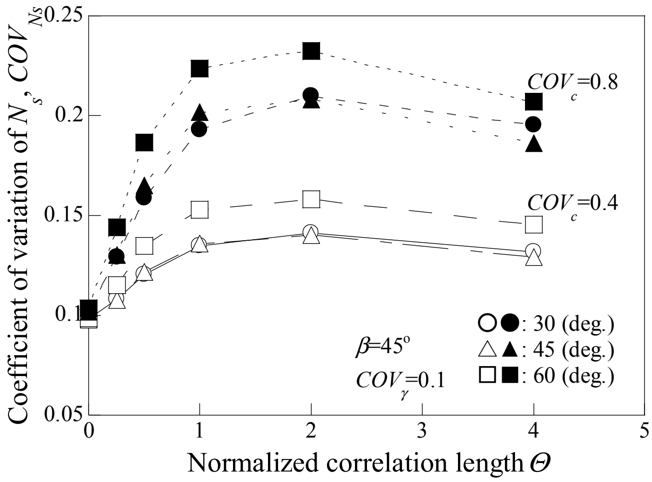

Figure 7 *COV* of stability number and normalized correlation length.

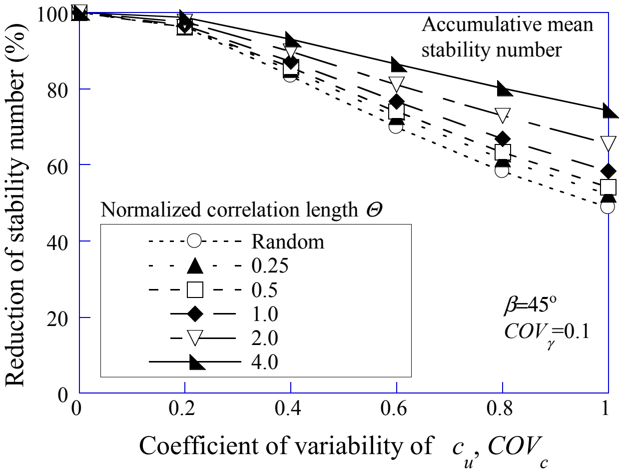

Figure 8. Reduction of stability number due to COV_c for a given Θ.

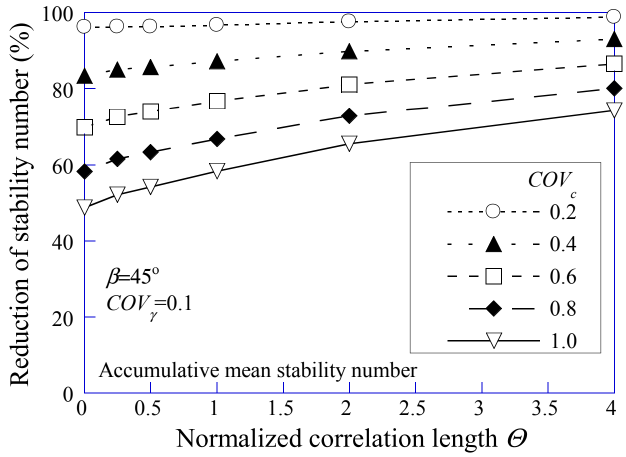

a) Accumulative mean stability number

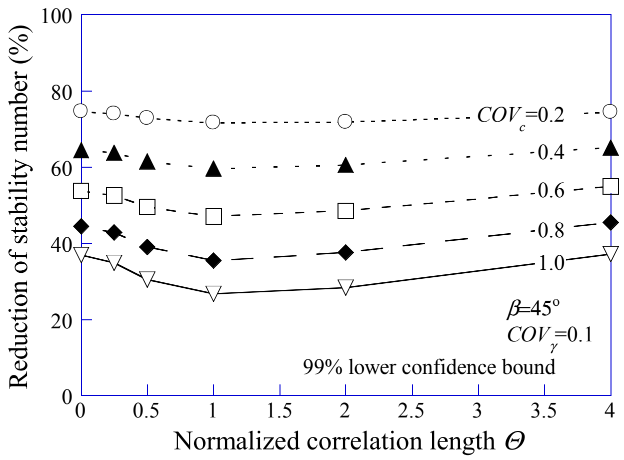

b) 99% lower confidence bound of stability number

Figure 9. Reduction of stability number due to Θ for a given COV_c.

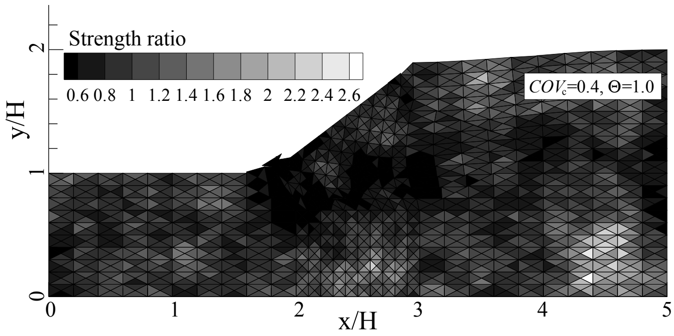

a) Deformed mesh

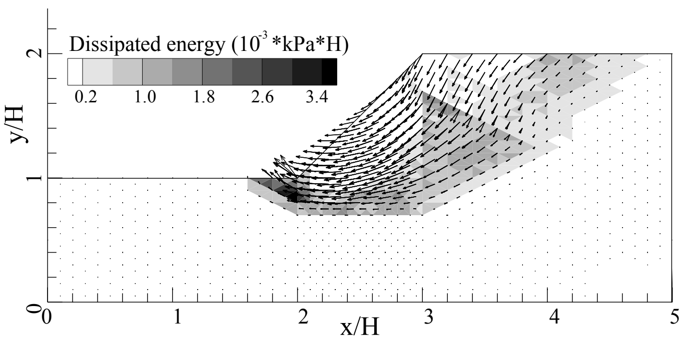

b) Dissipated energy and displacement vector

Figure 10. Typical failure mechanism.

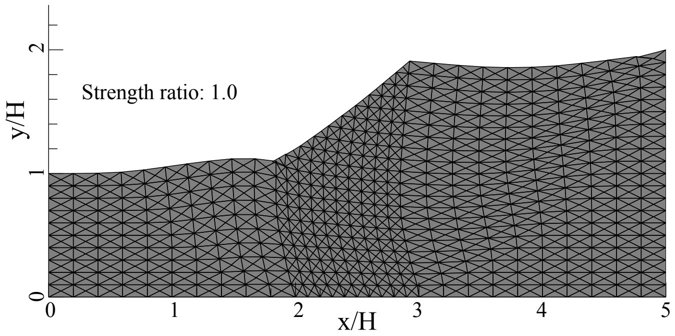

a) Deformed mesh

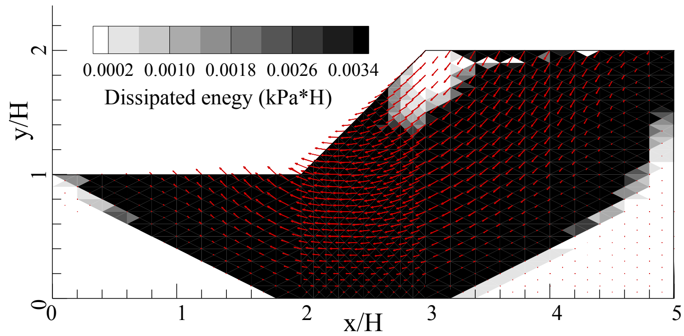

b) Dissipated energy and displacement vector

Figure 11. Failure mechanism for slope with uniform strength and unit weight.

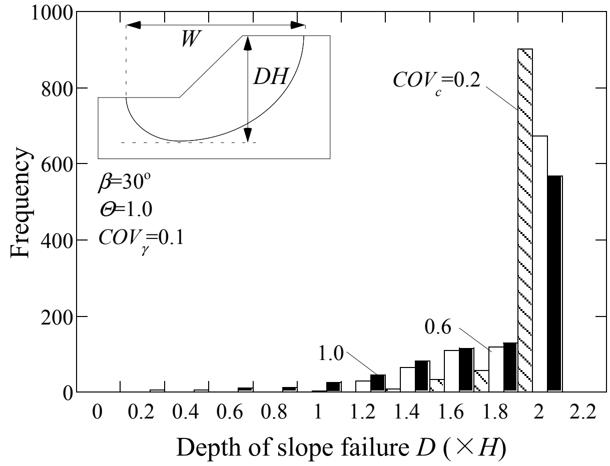

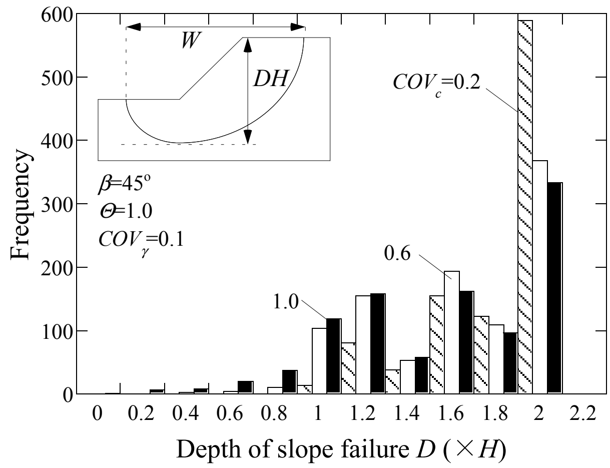

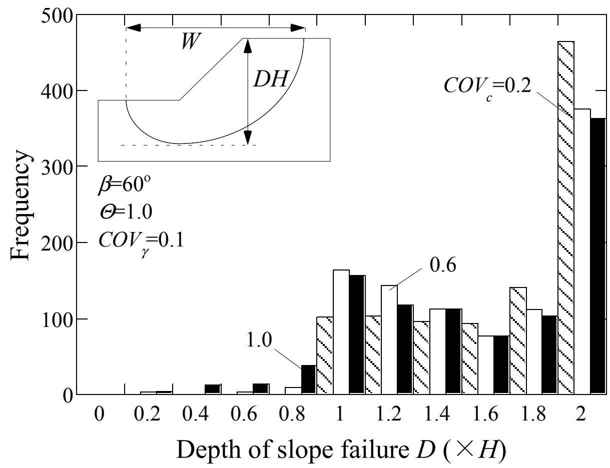

a) The depth of collapsed slope for a given β

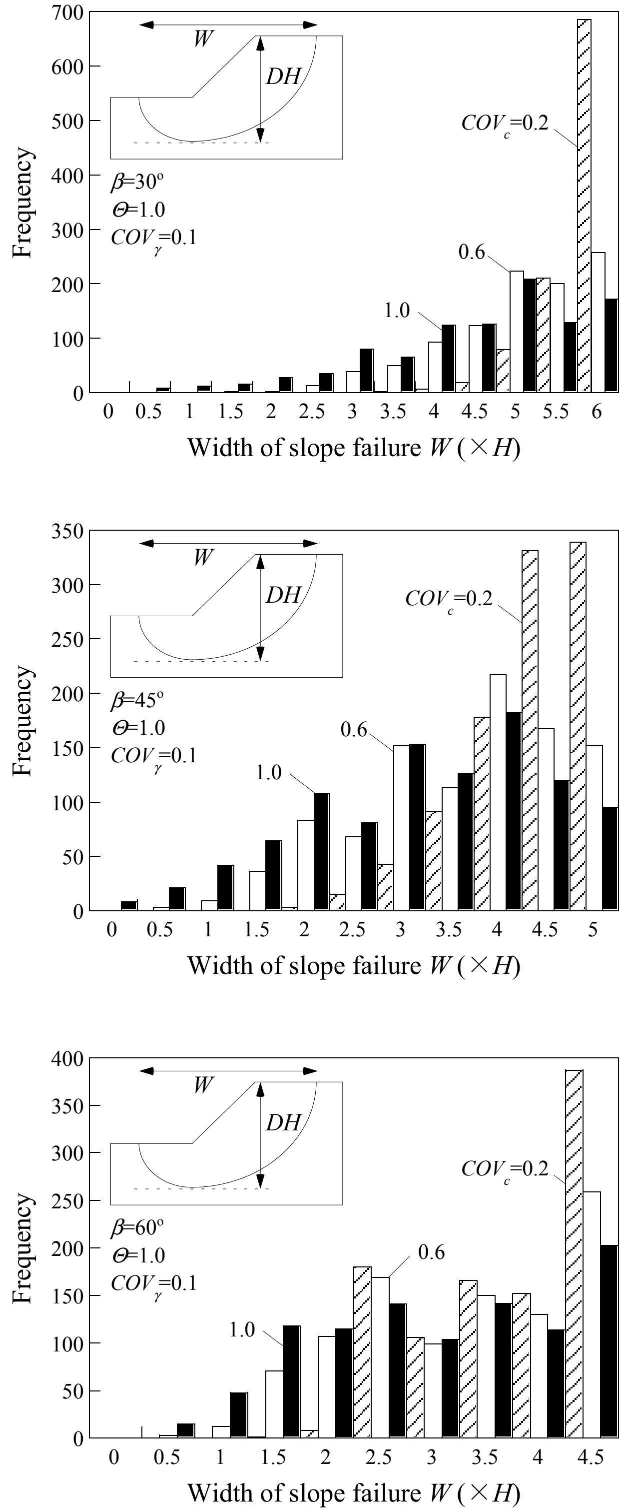

b) The width of collapsed slope for a given β

Figure 12. Histogram of the dimension of collapsed slope.

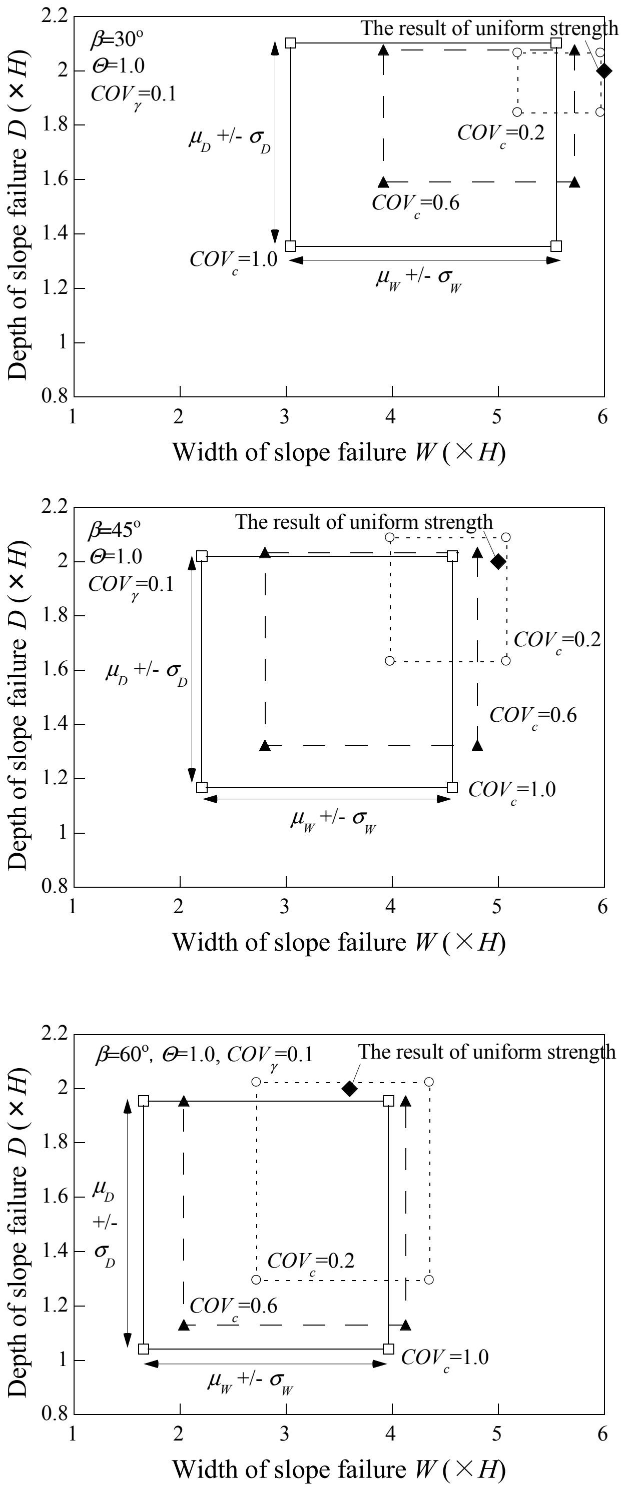

Figure 13. The relationships between the depth and width for collapsed slope for a given β.

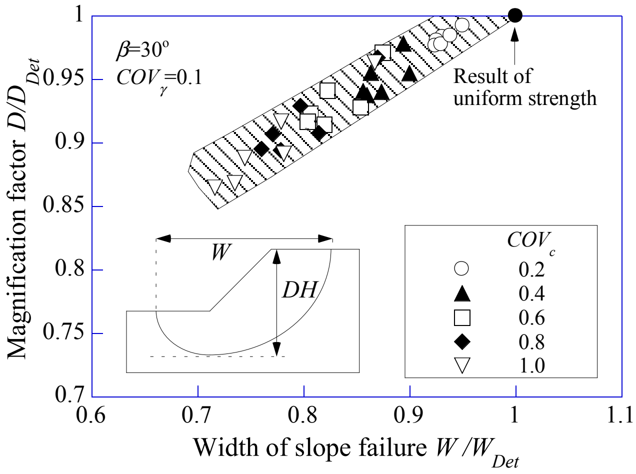

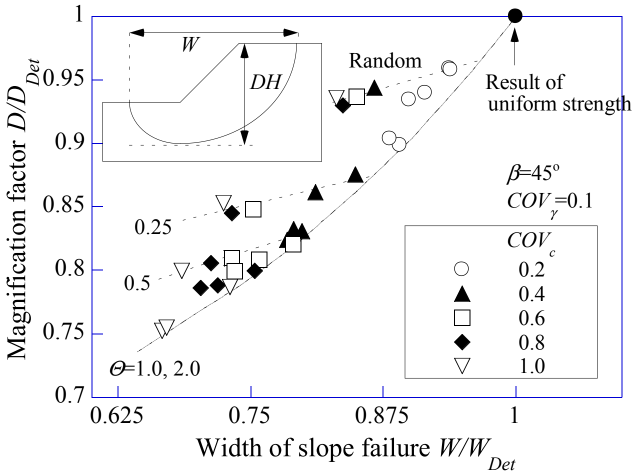

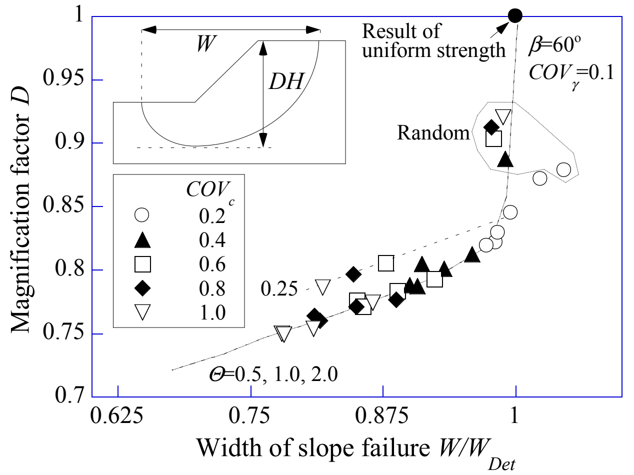

Figure 14. Relationships between width and depth of failure slope for a given β.

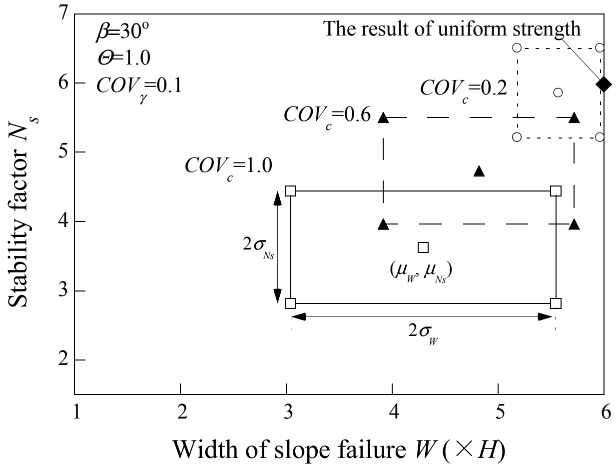

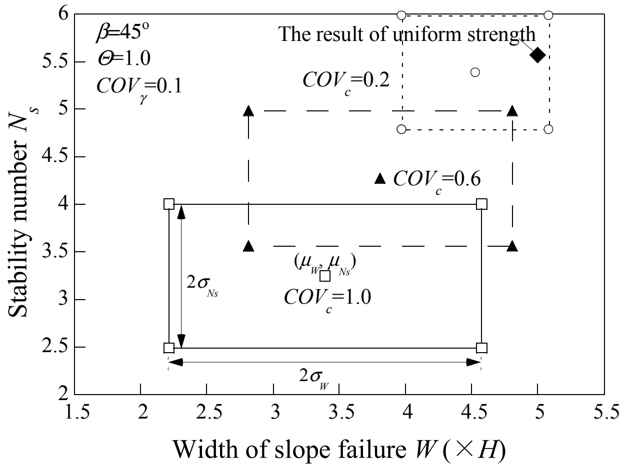

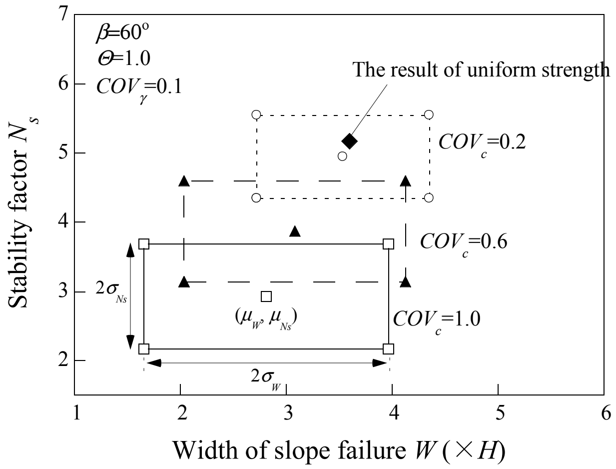

Figure 15. Stability number for slope and width of slope failure for a given β.

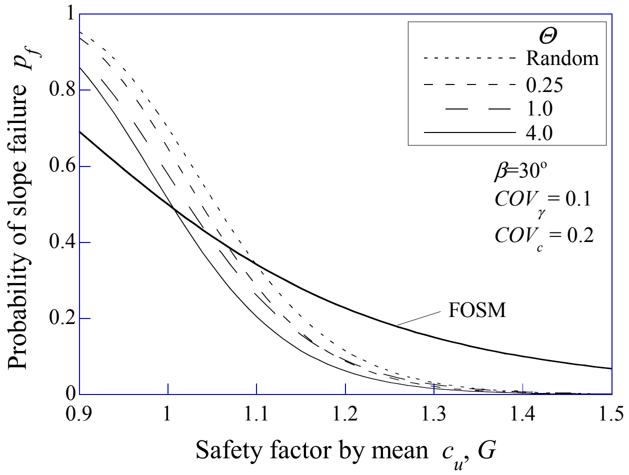
Θ
Random
0.25
1.0
4.0
β=30°
COVγ = 0.1
COVc = 0.2
FOSM
Probability of slope failure pf
Safety factor by mean cu, G
0
0.2
0.4
0.6
0.8
1
0.9
1
1.1
1.2
1.3
1.4
1.5

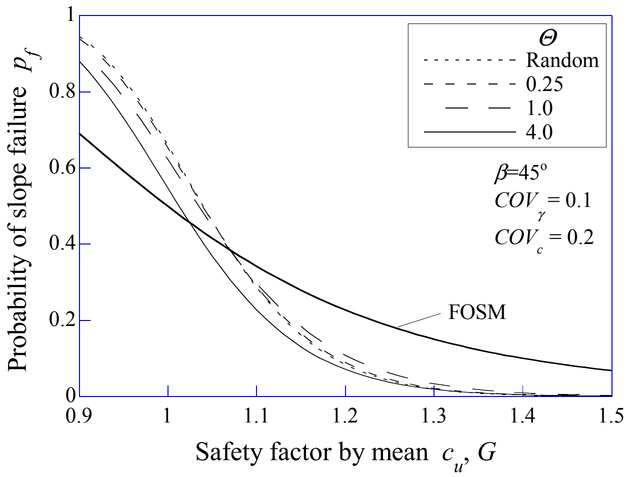
Θ
Random
0.25
1.0
4.0
β=45°
COVγ = 0.1
COVc = 0.2
FOSM
Probability of slope failure pf
Safety factor by mean cu, G
0
0.2
0.4
0.6
0.8
1
0.9
1
1.1
1.2
1.3
1.4
1.5

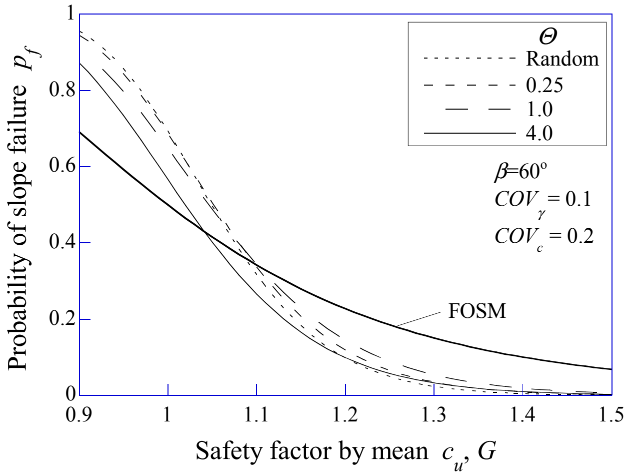
Θ
Random
0.25
1.0
4.0
β=60°
COVγ = 0.1
COVc = 0.2
FOSM
Probability of slope failure pf
Safety factor by mean cu, G
0
0.2
0.4
0.6
0.8
1
0.9
1
1.1
1.2
1.3
1.4
1.5

a) $COV_c = 0.2$

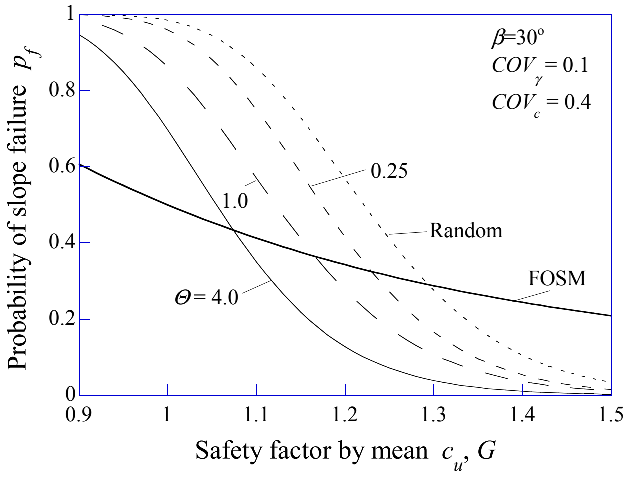

β=30°
COVγ = 0.1
COVc = 0.4
0.25
1.0
Random
FOSM
Θ = 4.0
Probability of slope failure pf
Safety factor by mean cu, G
0
0.2
0.4
0.6
0.8
1
0.9
1
1.1
1.2
1.3
1.4
1.5

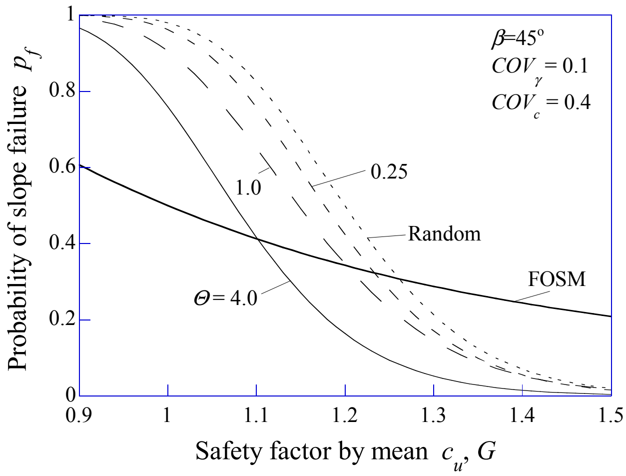

β=45°
COVγ = 0.1
COVc = 0.4
0.25
1.0
Random
FOSM
Θ = 4.0
Probability of slope failure pf
Safety factor by mean cu, G
0
0.2
0.4
0.6
0.8
1
0.9
1
1.1
1.2
1.3
1.4
1.5

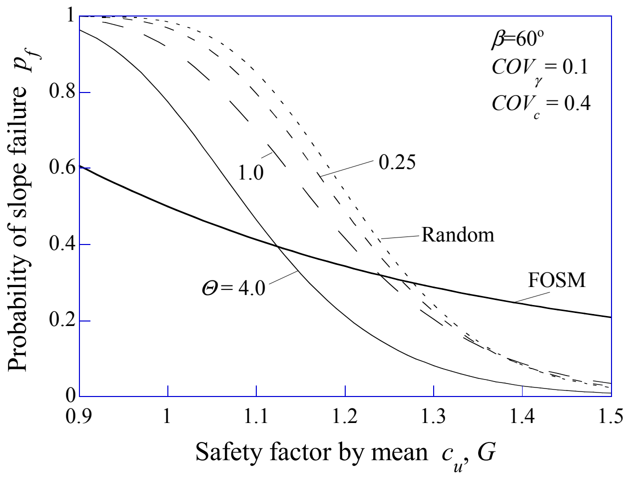

β=60°
COVγ = 0.1
COVc = 0.4
0.25
1.0
Random
FOSM
Θ = 4.0
Probability of slope failure pf
Safety factor by mean cu, G
0
0.2
0.4
0.6
0.8
1
0.9
1
1.1
1.2
1.3
1.4
1.5

b) $COV_c = 0.4$

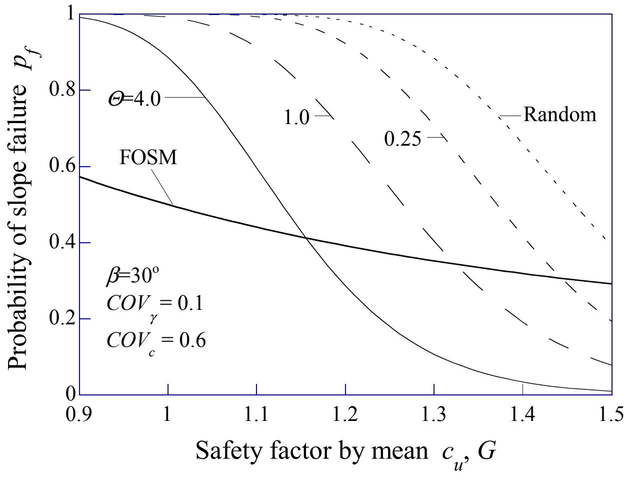

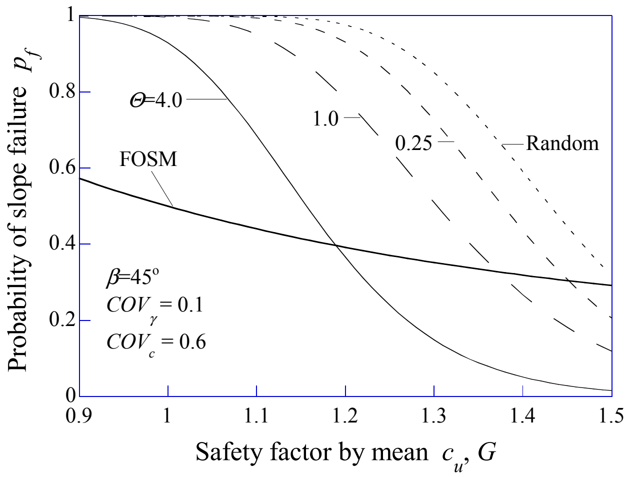

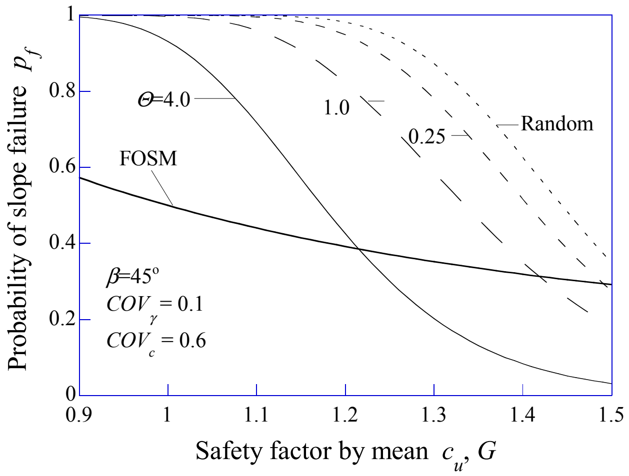

c) $COV_c = 0.6$

Figure 16. Probability of slope failure compared with FOSM for a given β.

Table 1. Input parameters.

Parameter	Value
Angle of slope	30^{o}, 45^{o}, 60^{o}
Mean undrained shear strength μ_c	100 kPa
Coefficient of variability of undrained shear strength, COV_c	0.2, 0.4, 0.6, 0.8, 1.0
Mean unit weight μ_γ	18 kN/m^3
Coefficient of variability of unit weight, COV_γ	0.1
Ratio of vertical and horizontal correlation length	1.0 (Isotropic)
Normalized correlation length $\Theta=\theta_c/H=\theta_\gamma/H$	Random, 0.25, 0.5, 1.0, 2.0, 4.0
Monte Carlo iterations	1000